Journal of Leather Science and Engineering

RESEARCH Open Access

The improvement of dispersity, thermal stability and mechanical properties of collagen fibers by silane modification: an exploration for developing new leather making technology

Shuangfeng Xu[1], Hanzhong Xiao[1] and Bi Shi[1,2*]

Abstract

The effect of hydrophobic modification on the performances of collagen fibers (CFs) was investigated by using silane coupling agents with different alkyl chains as hydrophobic modifiers. It was found silane could be easily grafted onto CF surface through covalent bonds under 5% water content. This modification led to the transformation of surface wettability of CF from hydrophilic to hydrophobic. Interestingly, the change of surface wettability resulted in substantial improvement of the modified CF properties, presenting well dispersity of collagen fibers, higher thermal stability and enhanced mechanical properties in comparison with natural CF. The degree of improvement mainly depended on the length of alkyl chain in silane. Longer alkyl chain produced strong hydrophobicity and subsequently more superior performances of the modified CF. When the length of alkyl chain increased to 18 carbon atoms, the modified CF possessed durable superhydrophobicity even exposed to aqueous solutions of different pH, UV, and organic solvents, and had excellent thermal and mechanical properties like leather fibers. In general, this work clearly revealed that the properties of CF are closely and positively related to the hydrophobicity, which is suggestive in developing new leather making technology.

Keywords: Hydrophobic modification, Collagen fibers, Silane, New leather-making technology

*Correspondence: sibitannin@vip.163.com

[1] Department of Biomass Chemistry and Engineering, Sichuan University, Chengdu 610065, People's Republic of China
Full list of author information is available at the end of the article

Graphical Abstract

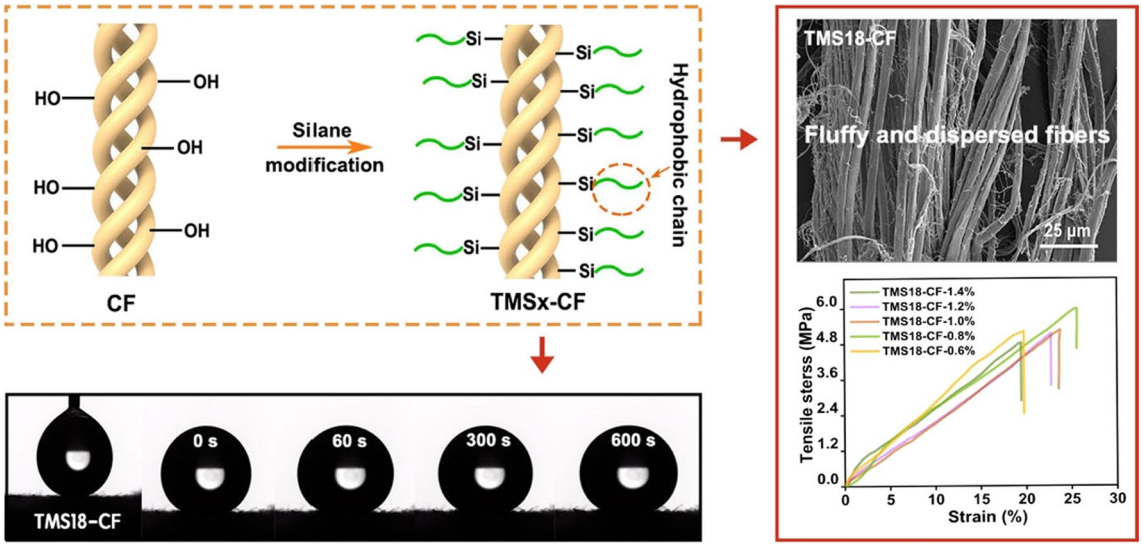

1 Introduction

For thousands of years, leather is converted from hides or skins by introducing additional crosslinks among CFs by various tanning agents [1]. Chrome tanning agent stands out among various tanning agents and imparts leather with high thermal stability and exceptional physical and mechanical properties [2]. However, chromium-containing wastewater and solid wastes may bring about environmental issues and human health risks [3–5]. Subsequently, to facilitate the green and sustainable leather industry, various chrome-free tanning technologies have been developed [6–11]. Inspired by strong chemical cross-linking between Cr (III) and CFs, the emphasis is usually focused on enhancing the chemical cross-linking between tanning agents and CFs in developing chrome-free tanning. But the fact is that the overall performances of chrome-free tanned leathers are inferior to chrome-tanned leather although some chrome-free tanning agents have strong reactivity with CFs. Therefore, it is worth considering that the performance of leather may not only depend on chemical cross-linking.

Rawhides are essentially hydrophilic materials with poor thermal stability, mechanical properties, and aesthetic properties as tanned leather. So far, little attention has been paid to the change in the wettability of the leather surface after tanning. We found that tanning, as a process to form chemical crosslinking, also put a significant impact on the surface wettability of leather. For example, the water contact angle (WCA) of the vegetable-tanned leather surface was 93°, and it took 30 s for water droplets to fully infiltrate [12], which implies the conversion of the leather surface from hydrophilic to temporary hydrophobic. The sheepskins tanned by aluminum and zirconium are also temporarily hydrophobic, with a WCA of 105° falling to 0° within 60 s [13]. Chrome-tanned leather behaves more prominent hydrophobicity. Xia et al. found that the WCA of chrome-tanned leather was 96.3°, which decreased to 0° at 300 s [14]. Zhu et al. also confirmed that the WCA of chrome-tanned leather was 108° without decreasing significantly in a short time [15]. The excellent overall performance of chrome-tanned leather may be closely related to its superior hydrophobicity. It is well known that leather tanning is also a process of converting the surface wettability of skins from hydrophilic to hydrophobic [16], and the essence of tanning might be attributed to the enhancement of hydrophobicity of collagen fibers.

Kayaoğlu et al. reported the plasma deposition of hexamethyldisiloxane on the surface of natural leather imparting leather with hydrophobicity and easy-care characteristics to prevent soiling and staining [13]. But the effect of hydrophobicity on the performance of natural leather had not been investigated in the research. He et al. fabricated a superhydrophobic coating on the surface of a dehydrated pelt by combining in-situ growth of TiO_2NPs and polydimethylsiloxane (PDMS) coating, and found that the superhydrophobic coating improved the water repellency of the dehydrated pelt and prevented it from reabsorbing water, so that the obtained untanned leather exhibited comparable physical properties to

chrome-tanned leather [17]. Sun et al. [18] investigated the influence of the hydrophobic chain length of gemini polyurethane surfactants in retanning system on the mechanical properties of aldehyde tanned leather. It was found that the elongation and tear strength of leather were increased by 14.5% and 18.4% respectively, when the hydrophobic chain length was 8 carbon atoms. In addition, the hydrophobic treatment of cationic silicon-based gemini surfactants with hydrophobic chains was beneficial to fiber dispersion of sheepskin [19]. To date, systematic investigation on how hydrophobicity affects the thermal stability, fiber dispersity, and mechanical properties of skin collagen fibers has not been reported. The profoundly understanding the role of hydrophobicity on the overall performances of collagen fibers is particularly significant, which may furnish a novel strategy for leather manufacturing.

In this work, CFs were used as the model of skin pelt to explore the method of hydrophobic modification, so as to prevent the influence of penetration of hydrophobic material in pelt on this theoretical exploration. The hydrophobic effect of CFs modified by silane coupling agents with different hydrophobic chain lengths was investigated. The hydrophobic durability, water absorption, dispersibility, thermal stability, and mechanical properties of modified CFs were investigated.

2 Experimental

2.1 Materials

Pickled cowhide pelt was provided by a local tannery in China. Dodecyltrimethoxysilane (TMS12, 93%), hexadecyltrimethoxysilane (TMS16, 85%) and octadecyltrimethoxysilane (TMS18, 90%) were obtained from Aladdin Co., Ltd. (Shanghai, China). Ethanol (95 wt%), isopropanol (99.7 wt%), NaCl (99.5%), $NaHCO_3$ (99.8%), HCOOH (88%), and other chemicals were supplied by Kelong Co., Ltd. (Chengdu, China). All chemicals used are analytical reagents.

2.2 Fabrication of dehydrated collagen fibers (CFs)

Anhydrous ethanol was used as a polar solvent to dehydrate the pelt. Pickled pelt was deacidified to pH 6.0 according to the conventional method and then was immersed into a drum with 150 wt% absolute ethanol. The drum was rotated for 2 h at a speed of 20 r/min. Then the pelt was taken out and the ethanol in the drum was recycled. This dehydration process was repeated for 5 times. Dehydrated pelt was obtained by drying at 35 °C for 12 h to completely volatilize ethanol. Then the dehydrated pelt was cut into small pieces (about 1 cm × 1 cm) with scissors, and crushed and sieved with an ultracentrifugal pulverizer (Retsch ZM200, Germany) with a sieve of 0.5 mm to obtain CFs of 30–40 mesh.

2.3 Fabrication of hydrophobic collagen fibers (TMSx-CF)

5 g of dehydrated CFs were firstly immersed into 50 ml of isopropanol solutions containing 0.8 w/v% of TMS12/ TMS16/ TMS18 respectively for 2 h under room temperature. Then 5 wt% of H_2O was added, and shaken for 12 h at 220 rpm. Finally, hydrophobic collagen fibers (TMSx-CFs, x stands for 12, 16 or 18) were obtained after drying at 105 °C for 4 h, which were named as TMS12-CF, TMS16-CF, and TMS18-CF. For comparison, silane content i.e. (0.6–1.4 w/v%) and water content (0–25 wt%) were adjusted. Siloxane content (w/v%) refers to the percentage of the mass of siloxane relative to the volume of isopropanol, and water content (wt%) is the mass percentage of water and CFs.

2.4 Characterization

The chemical composition of samples was monitored by a NICOLET iS10 FTIR spectrometer (Thermo Fisher Scientific, USA) at a resolution of 4 cm^{-1} and in the range of 4000–500 cm^{-1}. The mass loss of samples in heating was characterized by a synchronous thermal analyzer (TG, Q600, TA) from 30 to 800 °C with a heating rate of 10 °C/min. In order to analyze the chemical composition in detail, the binding energies of the elements were investigated by X-ray photoelectron spectroscopy (XPS; Thermo Scientific, NEXSA). An OXFORD DULTIM MAX energy spectrum analyzer was used to detect the surface chemical elements of samples. The morphology of samples was observed through a field-emission scanning electron microscope (FESEM; Nova Nano- SEM450, FEI) at a voltage of 5 kV. The water contact angles (WCAs) were measured using a contact angle goniometer (Krüss, DSA30, Germany) with 5 μl of water, and the obtained values were the averages of five parallel measurements. Shrinkage temperature of collagen fibers was analyzed in the heating mode of a thermostatic workbench from 30 to 200 °C with a heating rate of 10 °C/min, and the fiber length change with temperature was recorded under a stereomicroscope (Super depth of field 3D microscopic system, VHX5000). The mechanical properties of collagen fibers were measured by an electronic single fiber strength meter (Laizhou Electronic Instrument Co., Ltd., LLY-06B, China).

3 Results and discussion

The conversion of collagen fiber wettability from hydrophilic to hydrophobic is attributed to two key factors: the roughness of the hierarchical structures and the low surface energy substance [20, 21]. Without additional

roughness construction, the enhancement of hydrophobicity of collagen fiber mainly relies on its own rough hierarchical structures and the chemical modification of long-chain silane coupling agents. In this research, TMS12, TMS16, and TMS18 with long-chain alkyl were chosen to hydrophobically modify CFs. The hydrophilic head of (–Si(OCH_3)$_3$) is hydrolyzed to generate –Si–OH groups [22], which can connect with the –OH of CFs by hydrogen bond and covalent bond through dehydration reaction (Fig. 1). Hydrophobic TMSx-CFs were obtained by covalently grafting [23] the hydrophobic long-chain hydrocarbon tail (–Si–$(CH_2)_{x-1}CH_3$) of TMS12, TMS16, and TMS18 on CFs. Due to the inherent hydrophilicity of CFs, water droplets could be completely spread out on the surface of the CFs and be absorbed rapidly, and swelling behavior happened when the CFs was immersed in water. On the contrary, silver mirror reflection was observed when TMS12-CF, TMS16-CF, and TMS18-CF were immersed in water (Additional file 1: Fig. S1), revealing their non-wetting Cassie-Baxter surface [24].

To verify the covalent bonds formed between TMSx and CFs, FTIR spectroscopies of pristine CFs and TMSx-CFs were displayed in Fig. 2a. The enhanced peak at 1086 cm^{-1} confirms the presence of Si–O–Si [25] and the new sharp transmission bands at 2850 and 2929 cm^{-1} are attributed to the symmetric and asymmetric stretching vibrations of $–CH_2$ and $–CH_3$ [26], which proves the successful grafting of silane coupling agents as compared with the pristine CFs. Obviously, longer alkane chain of TMSx led to stronger $–CH_2$/$–CH_3$ peak. The TGA and DTG curves of the samples from room temperature to 800 °C under N_2 were shown in Fig. 2b, c. TGA curves demonstrated that the decomposition curves of the samples were similar. The residual mass and maximum decomposition temperature of TMS12-CF, TMS16-CF and TMS18-CF were all higher than those of CF. The maximum decomposition temperature of TMSx-CFs increased with the increase of the hydrophobic chain length of TMSx. The maximum decomposition temperature of TMS18-CF was 365 °C, which was 5 °C higher than TMS12-CF and 8 °C higher than CF. These results indicated the successful attachment of silane coupling agents on the surface of CFs through covalent bonds [27], and implicated that a stronger hydrophobicity of TMSx-CFs may lead to a higher thermal stability. Energy dispersive spectroscopy (EDS) analysis was performed to assess the chemical composition of TMSx-CF. As shown in Fig. 2d, the peak of Si was detected on TMS12-CF, TMS16-CF, and TMS18-CF other than C, N, and O. The element Si and a part of element C were mainly derived from TMSx, while N, O, and a part of C came from CF. As an illustration in Fig. 2d, compared with CF, the C content of TMSx-CF increased due to the existence of long-chain alkanes, which suppressed the N content. In addition, the values of C/N, C/O and Si content increased with increasing chain length of alkanes, further confirming that CFs were well modified by TMSx. The XPS spectra of the samples were shown in Fig. 2e. TMS12-CF, TMS16-CF and TMS18-CF were all composed of the clear signal peaks of C, N, O and Si elements. The C 1 s peaks in TMS12-CF, TMS16-CF and TMS18-CF were much higher than that in CF due to the existence of long alkane chain in TMSx, so that the relative strength of O1s and N1s was lower than that of CF, which is consistent with the results of EDS. The C1s area of CF can be divided into three Gaussian curve peaks located at 284.4, 285.6 and 287.5 eV, representing C–C, C–O–C, and C=O, respectively. The C1s area of TMS12-CF, TMS16-CF and TMS18-CF can be divided into four Gaussian curve peaks appeared at 284.4, 285.2, 286.5 and 288.1 eV, separately attributed to C–C, C–O–Si, C–O–C, and C=O [28], where the new peak of C-O-Si demonstrated

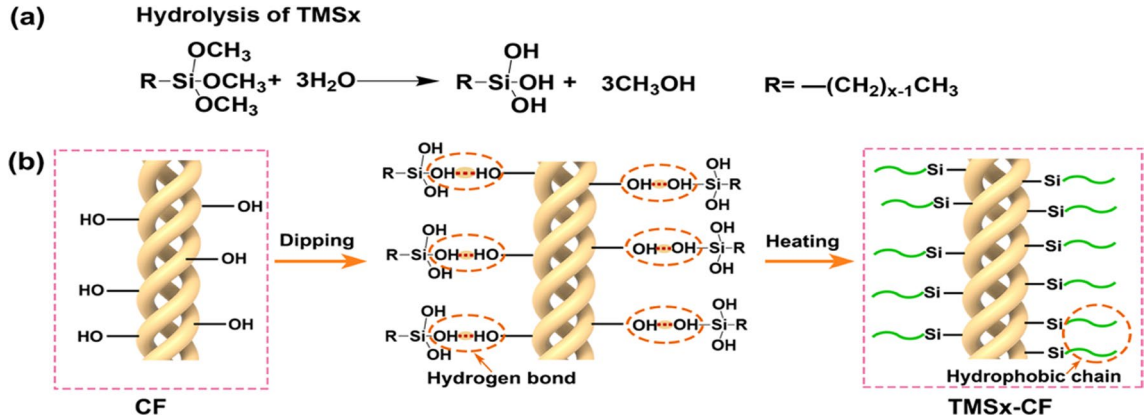

Fig. 1 Schematic illustration showing the fabrication of TMSx-CF

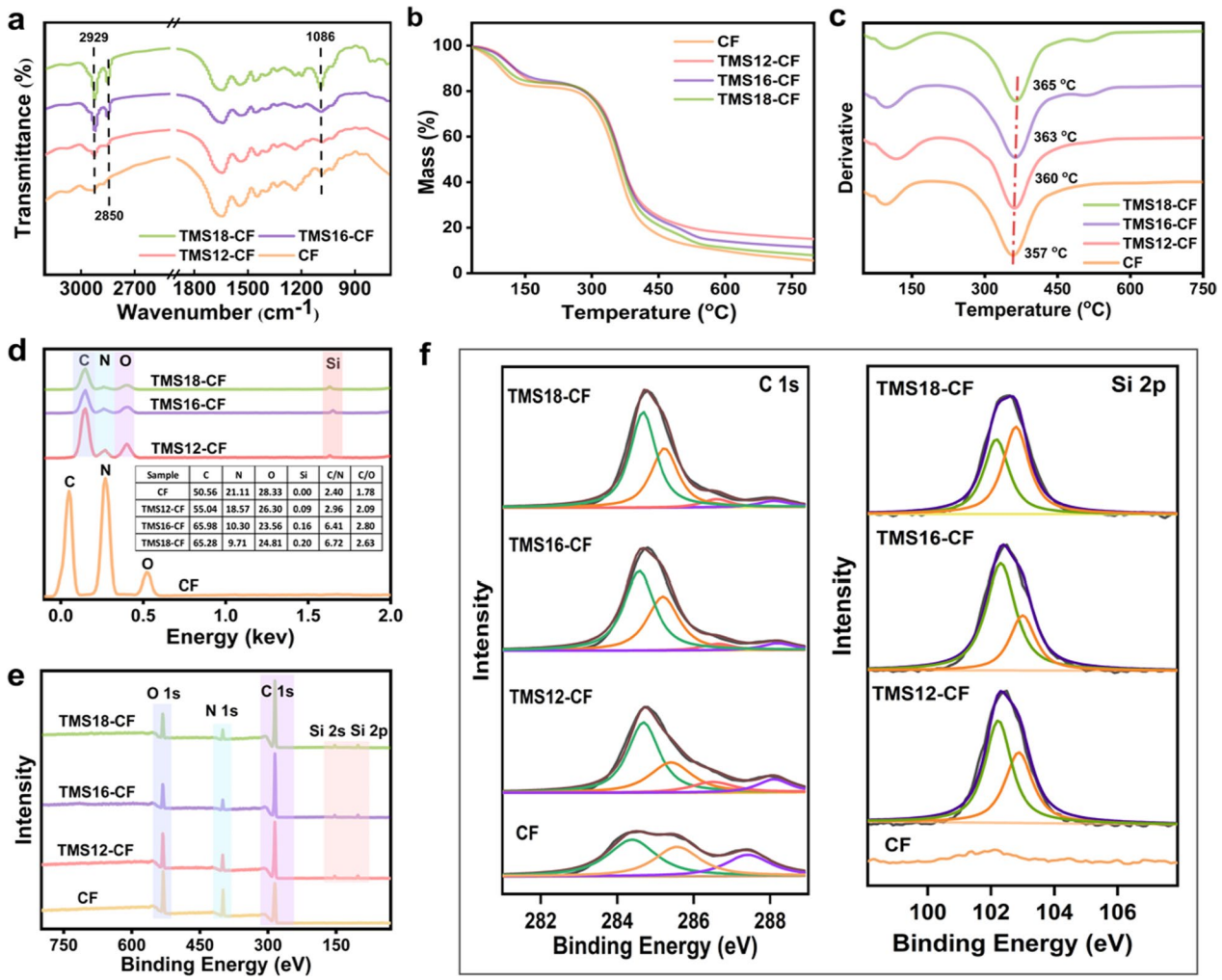

Sample	C	N	O	Si	C/N	C/O
CF	50.56	21.11	28.33	0.00	2.40	1.78
TMS12-CF	55.04	18.57	26.30	0.09	2.96	2.09
TMS16-CF	65.98	10.30	23.56	0.16	6.41	2.80
TMS18-CF	65.28	9.71	24.81	0.20	6.72	2.63

Fig. 2 Fourier transform infrared spectra (**a**), TGA curves (**b**), DTG curves (**c**), EDX spectra (**d**), XPS spectra (**e**), XPS C 1 s and Si 2p spectra (**f**) of CF, TMS12-CF, TMS16-CF and TMS18-CF

the formation of covalent bonds between silane and CFs. In addition, the Si 2p region of TMS12-CF, TMS16-CF and TMS18-CF can be split into two Gaussian curves peaks at 102.2 and 102.9 eV, which belonged to Si–O and Si–C [29]. XPS analysis suggested the formation of covalent bonds between CFs and TMSx, and the presence of long-chain alkanes in TMSx-CFs, which were in accordance with the results of FTIR, EDS and TG-DTG. These results strongly confirmed that silane is covalently bonded to CFs, which ultimately endow TMSx-CFs with enhanced hydrophobicity.

Then, the hydrophobicity of TMSx-CFs was optimized by adjusting the contents of silane coupling agents and water in TMSx-CFs. The effect of silane content on the hydrophobicity of TMSx-CFs was firstly investigated. As shown in Fig. 3a, with the increase of silane content, the WCAs gradually increased and then decreased. The higher silane content led to the lower surface energy and therefore, improved water repellency of TMSx-CFs. When the silane content was higher than 1%, the WCAs of the TMSx-CFs reduced, suggesting the reduction of water resistance. The explanation may be that long-chain alkyl groups with lower surface energy were mainly grafted onto the surface of CFs [30], and excess silane would self-condense to form polymers that wrapped around CFs, destroying the hierarchical structure of CFs, thereby bringing about diminished surface roughness and decreased hydrophobicity. Therefore, an excessively high content of silane may not contribute to a further decrease of surface energy, and the hydrophobicity of the TMSx-CFs decreased instead. The influence of water content on the hydrophobicity of TMSx-CFs was also analyzed. It can be seen from Fig. 3b that, compared with the anhydrous system, the WCAs of TMSx-CFs increased with

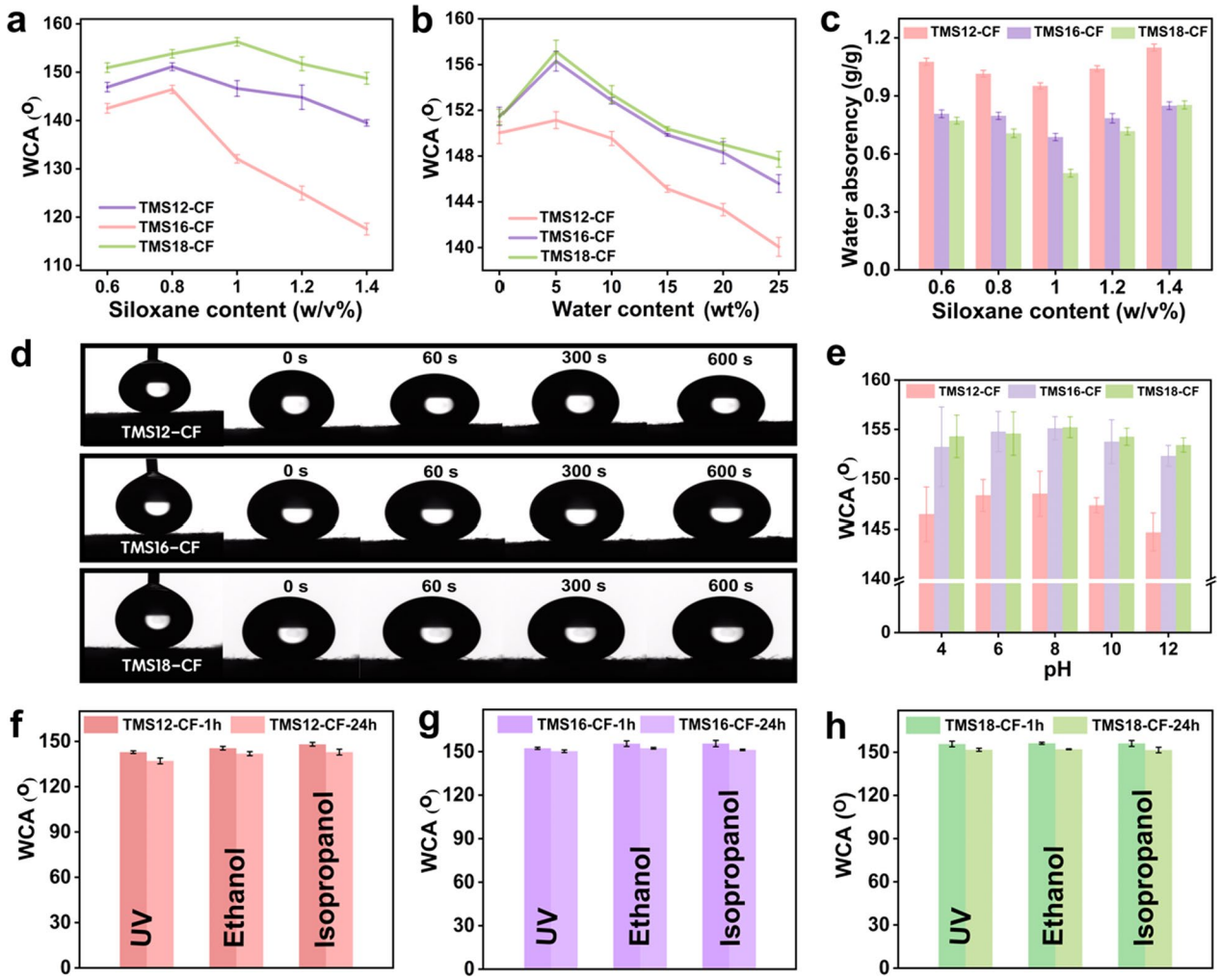

Fig. 3 WCAs of TMSx-CF with different silane content (**a**), WCAs of TMSx-CF with different water content (**b**), Water absorbency of TMSx-CF with different siloxane content (**c**), the shape of a water droplet on the TMS12-CF, TMS16-CF, TMS18-CF samples at different times (**d**), WCAs of the TMSx-CF treated by immersion in different pH solutions for 24 h (**e**), WCAs of the TMS12-CF (**f**), TMS16-CF (**g**), TMS18-CF (**h**) treated by UV for 1 h and 24 h, or immersion in various organic solvents for 1 h and 24 h

the addition of 5% water. This may be due to the sufficient hydrolysis of silane, which favors the formation of more binding sites with CFs, thereby improving hydrophobicity. When the water content exceeded 5%, WCAs decreased because the excess water is more likely to form hydrogen bonds with the hydroxyl groups, preventing the silane from binding to CFs. For all the TMSx-CFs, the WCAs first increased and then decreased with increasing content of silane coupling agents and water. WCAs of TMSx-CFs were also influenced by alkyl chain length of TMSx. As presented in Fig. 3a, b, the WCA of TMSx-CF raised with growing alkyl chain length. The optimal WCA of TMS12-CF was about 149.5°, indicating its hydrophobic surface. The surfaces of TMS16-CF and TMS18-CF were superhydrophobic, since their optimized WCAs reached around 156°. The water absorption of TMSx-CFs presented the opposite trend against their hydrophobicity. As the content of the silane coupling agent raises, the overall water absorption rate of hydrophobic TMS12-CF was higher than 0.95 g/g, while the water absorption rate of superhydrophobic TMS18-CF was as low as 0.5 g/g (Fig. 3c), revealing that the enhanced hydrophobicity effectively inhibited the water absorption. The inhibition of water absorption also relied on the length of the alkyl chain. Water absorption of TMS18-CF was significantly lower than that of TMS12-CF because the longer alkyl chain could provide lower surface energy and enhanced hydrophobicity.

In order to investigate the hydrophobic stability of the samples, the shape of the water droplets at different times

on the TMSx-CF surface was taken. The hydrophobicity of TMS12-CF was unstable, and the water droplet gradually infiltrated within 600 s. When the alkyl chain length raised to 16 and 18, TMS16-CF and TMS18-CF presented stable superhydrophobicity, the WCAs of which were higher than 150° at 600 s, and no significant infiltration occurred. Then, the chemical durability of hydrophobicity was further evaluated by recording the variations of WCAs over time when TMSx-CF were exposed to various conditions. Samples were immersed in aqueous solutions of different pH (pH = 4–12) for 24 h (Fig. 3e). WCAs of TMS12-CF under acid or alkali conditions were significantly lower than that under pH = 8. But the WCAs of TMS16-CF and TMS18-CF only slightly changed in the pH range of 4–12, suggesting strong resistance to pH. The silver mirror reflection phenomenon was also found on the surface of TMS16-CF and TMS18-CF soaked in aqueous solution with different pHs (Additional file 1: Fig. S2), further reflecting their durable water resistance. This phenomenon may be attributed to the fact that the air layer trapped between the interfaces of superhydrophobic collagen fibers and water can resist acid or alkali corrosion. In addition, when samples were irradiated with UV for 1 h and 24 h or soaked into ethanol and isopropanol for 1 h and 24 h, the WCAs of TMS16-CF and TMS18-CF did not change a lot and maintained at about 150°. These results demonstrated that the long alkyl chain combined with CFs endowed TMS16-CF and TMS18-CF with durable and stable water repellency enough to resist the complex external environment, including UV, pH, and various polar solvents.

In order to monitor the fiber dispersity and morphological differences of TMSx-CFs, SEM images with different magnifications were taken. It can be seen from Fig. 4a that TMS12-CF, TMS16-CF, and TMS18-CF were all composed by nanoscopic fibril and microscopic fiber [31]. There were a small amount of pores between the microfibers.

and nanofibers of TMS12-CF. But, as the hydrophobic chain length increased, porosity among microfibers and nanofibers increased, presenting more fluffy and dispersed fibers in TMS16-CF and TMS18-CF. This implied that longer hydrophobic chains promoted fiber dispersity of CFs more effectively. The fiber dispersity of hydrophobic collagen fiber followed the order of TMS18-CF > TMS16-CF > TMS12-CF. Obviously, the degree of fiber dispersity of TMSx-CFs was positively correlated with their hydrophobicity because the WCAs of TMS18-CF and TMS16-CF were 158.3° and 155.9°, respectively, which was much higher than the 148.6° of TMS12-CF (Fig. 4b).

The denaturation temperatures of all the samples were measured by differential scanning calorimetry (DSC), and the shrinkage temperatures were recorded by monitoring the length change of the samples with increasing temperature. The thermal stability of TMSx-CF was

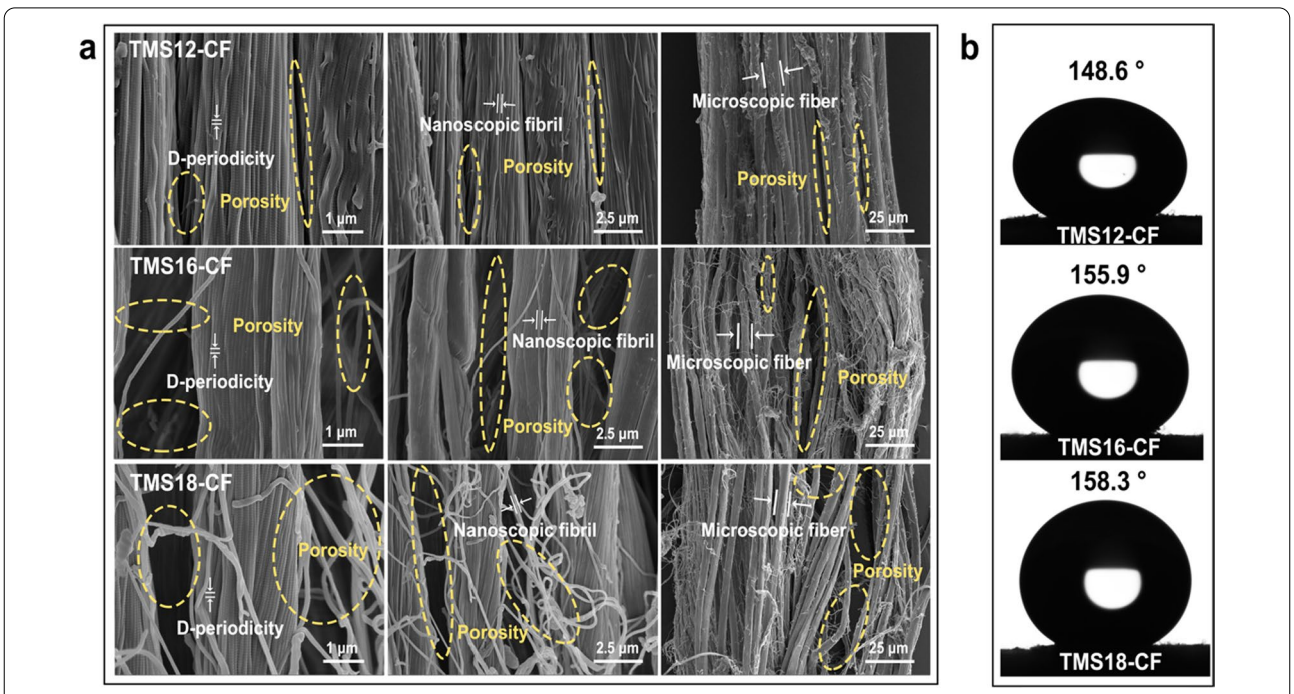

Fig. 4 SEM images of TMSx-CF (**a**), and WCAs of TMSx-CF (**b**)

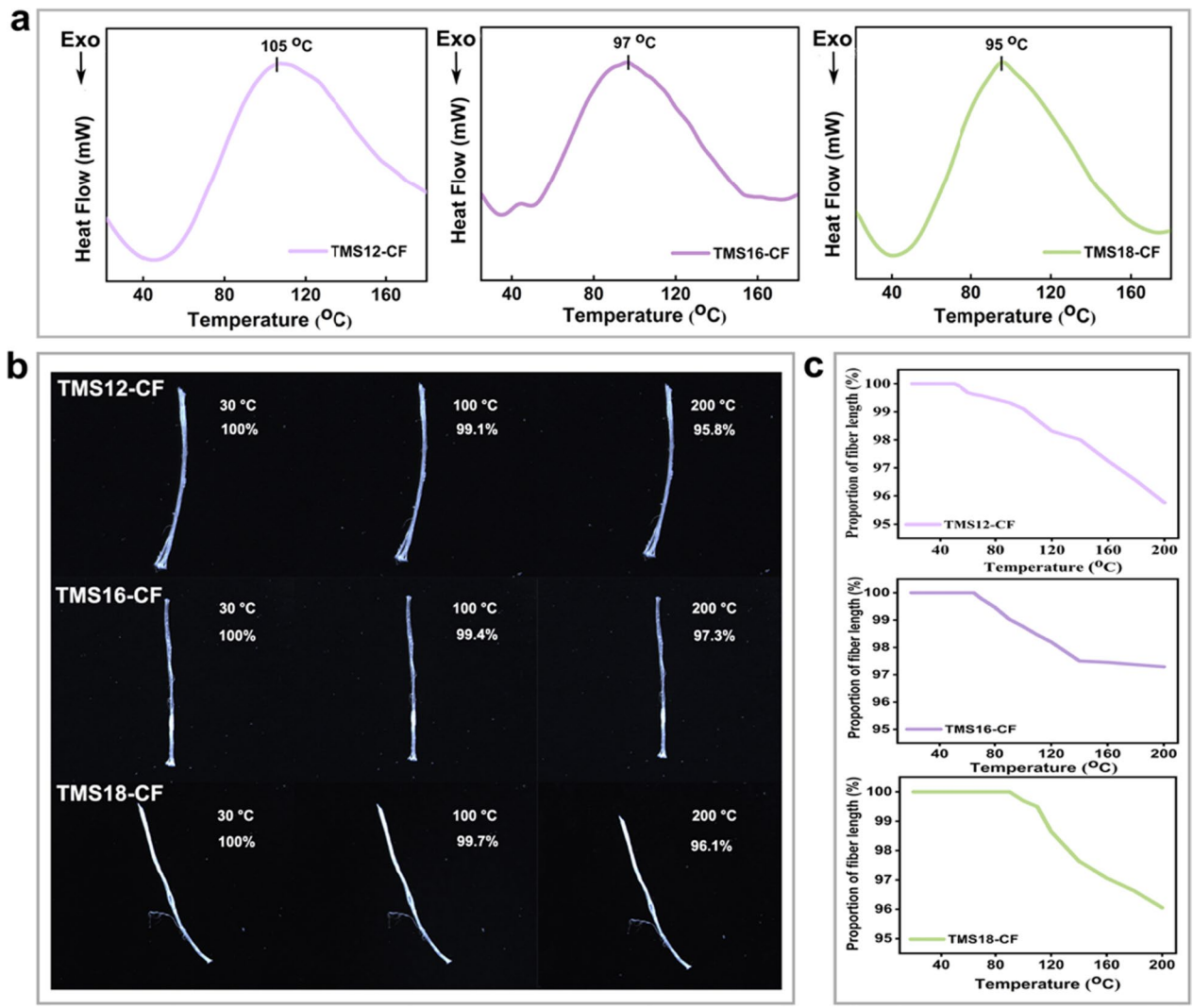

Fig. 5 DSC curves of TMSx-CF (**a**), digital photos of TMSx-CF at different temperatures (**b**), the length percentage of the TMSx-CF at different temperatures (**c**)

effectively improved. Additional file 1: Fig. S3 and Fig. 5a showed that the denaturation temperatures of TMS12-CF, TMS16-CF, and TMS18-CF were 41 °C, 33 °C, and 31 °C higher than CF, respectively. This phenomenon may be partly attributed to the covalent bonds formed between the silane coupling agent and CFs that facilitate the enhancement of thermal stability. Furthermore, with raising temperature, the shrinkage behavior of TMS12-CF was the most considerable, and its length at 100 °C was only 99.1% of its original length, while the lengths of TMS16-CF and TMS18-CF remained at 99.4% and 99.7% (Fig. 5b). Besides, it can also be seen from the fiber length percentage change curves over temperature that TMS16-CF and TMS18-CF had a wider thermostable plateau where there is no significant change in fiber length within 100 °C (Fig. 5c), showing more superior heat resistance than TMS12-CF. In general, the shrinking degree of TMSx-CFs under heating was in the order of TMS18-CF < TMS16-CF < TMS12-CF, demonstrating that silane coupling agents with longer hydrophobic chain endowed modified collagen fiber with better heat resistance.

Collagen fiber, a kind of biomaterial with a nano- to a micro-scale hierarchical structure [32], has good mechanical properties and can be bent at any angle [33]. TMSx-CFs, such as TMS12-CF, TMS16-CF, and TMS18-CF, owned better mechanical responses. This phenomenon may be related to the excellent fiber dispersion promoted by hydrophobic modification, which provided more space for inter- and intra-fibrillar sliding to accommodate the imposed strain [31], while hydrophobicity

played a lubricating role in sliding [34]. In addition, the covalent bond formed in hydrophobic modification played a positive role in stabilizing collagen fibers, which delayed intermolecular sliding, and allowed collagen molecules to further deform [35]. Therefore, compared with CFs, TMSx-CF have higher overall mechanical properties.

As shown in Fig. 6, the increase of hydrophobic chain length was conducive to the increase in tensile strength and elongation at the break. Obviously, the tensile strength and elongation at the break of TMS18-CF were significantly higher than those of TMS12-CF and TMS16-CF. The increased fracture energy of TMS18-CF also implied that it was more difficult to be broken. TMS12-CF with higher Young's modulus was more rigid

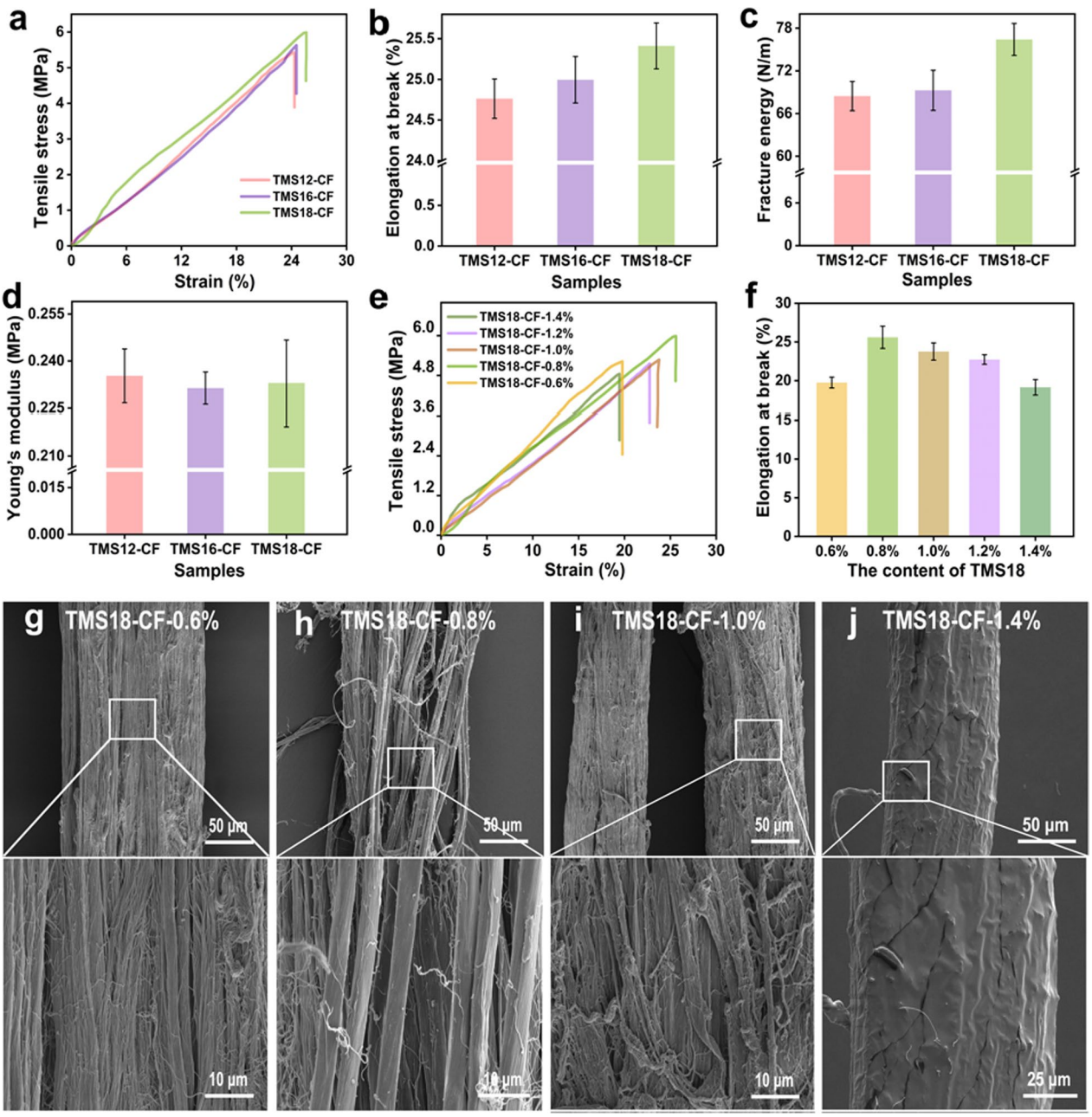

Fig. 6 Stress–strain curves (**a**), elongation at break (**b**), fracture energy (**c**), and Young's modulus (**d**) of different collagen fibers, stress–strain curves of TMS18-CF with different content of TMS18 (**e**), elongation at break of TMS18-CF with different content of TMS18 (**f**), SEM images of TMS18-CF-0.6% (**g**), TMS18-CF-0.8% (**h**), TMS18-CF-1.0% (**i**), TMS18-CF-1.4% (**j**)

than TMS16-CF and TMS18-CF, indicating that TMS16-CF and TMS18-CF were more flexible. The above results demonstrated that TMS18-CF possessed better flexibility than TMS16-CF and TMS12-CF. It can be also found that longer hydrophobic chains stimulated the enhancement of the mechanical properties of TMSx-CF, which should be due to the fact that the longer hydrophobic chain played a better lubricating effect on the movement behavior of collagen fibers. Besides, longer hydrophobic chain contributed to more effective dispersion of collagen fibers, being conducive to stress release, and improvement of elasticity and ductility.

Moreover, the effect of TMS18 content in TMS18-CF on its tensile strength was also evaluated. As shown in Fig. 6f, the highest tensile strength of TMS18-CF appeared at 0.8% TMS18 content. The SEM images (Fig. 6g–j) showed that the TMS18-CF with 0.8% TMS18 content possessed significantly well-dispersed fiber bundles. When the content of TMS18 was less than 0.8%, the dispersity of collagen fibers or fibrils was not good enough. When the content of TMS18 was higher than 0.8%, excessive TMS18 would self-condense [36] to form a coating on the surface of the fiber bundle which wraps the collagen fibers and fibrils, destroying their hierarchical structures. The poor fiber dispersity would restrict the slipping space of fiber bundles during stretching, which was the reason for worse mechanical properties. Therefore, a rational dosage of silane is important in developing satisfactory properties of collagen fibers.

4 Conclusions

The effect of hydrophobic modification on the performances of collagen fibers (CFs) has been investigated by using silane coupling agents with alkyl chain lengths of 12, 16, and 18 as hydrophobic modifiers. The surface wettability of collagen fibers can be changed from hydrophilicity to hydrophobicity through the modification, and the hydrophobicity and hydrophobic durability of the modified collagen fibers can be improved as the length of hydrophobic chain increases. Meanwhile, the hydrophobic modification can promote collagen fiber dispersity, remarkably improve the thermal stability and mechanical properties of collagen fibers, which may inspire the development of new tanning technology.

Supplementary Information

The online version contains supplementary material available at https://doi.org/10.1186/s42825-022-00100-8.

Additional file 1. Supplementary materials.

Acknowledgements
This work is financially supported by the National Natural Science Foundation of China (No. 21978176).

Author contributions
BS conceived the idea. SX carried out materials preparation. SX and HX carried out materials characterization. SX and BS drafted the manuscript. All authors analyzed the experimental results. All authors read and approved the final manuscript.

Funding
The National Natural Science Foundation of China (No. 21978176).

Availability of data and materials
All data from this study are presented in the paper and the supplementary material.

Declarations

Competing interests
The authors declare that there are no competing interests.

Author details
[1]Department of Biomass Chemistry and Engineering, Sichuan University, Chengdu 610065, People's Republic of China. [2]National Engineering Laboratory for Clean Technology of Leather Manufacture, Sichuan University, Chengdu 610065, People's Republic of China.

Received: 19 July 2022 Revised: 25 August 2022 Accepted: 31 August 2022
Published online: 14 September 2022

References

1. Covington AD. Tanning chemistry: the science of leather. Royal Society of Chemistry; 2009.
2. Zhang J, Chen W. A rapid and cleaner chrome tanning technology based on ultrasound and microwave. J Clean Prod. 2020;247:119452. https://doi.org/10.1016/j.jclepro.2019.119452.
3. Dixit S, Yadav A, Dwivedi PD, Das M. Toxic hazards of leather industry and technologies to combat threat: a review. J Clean Prod. 2015;87:39–49. https://doi.org/10.1016/j.jclepro.2014.10.017.
4. Kanagaraj J, Panda RC, Kumar MV. Trends and advancements in sustainable leather processing: future directions and challenges—a review. J Environ Chem Eng. 2020;8(5):104379. https://doi.org/10.1016/j.jece.2020.104379.
5. Rigueto CVT, Nazari MT, Rosseto M, Massuda LA, Alessandretti I, Piccin JS, Dettmer A. Emerging contaminants adsorption by beads from chromium (III) tanned leather waste recovered gelatin. J Mol Liq. 2021;330:115638. https://doi.org/10.1016/j.molliq.2021.115638.
6. Qiang T, Gao X, Ren J, Chen X, Wang X. A chrome-free and chrome-less tanning system based on the hyperbranched polymer. ACS Sustain Chem Eng. 2016;4(3):701–7. https://doi.org/10.1021/acssuschemeng.5b00917.
7. Krishnamoorthy G, Sadulla S, Sehgal PK, Mandal AB. Greener approach to leather tanning process: D-lysine aldehyde as novel tanning agent for chrome-free tanning. J Clean Prod. 2013;42:277–86. https://doi.org/10.1016/j.jclepro.2012.11.004.
8. Yu Y, Lin Y, Zeng Y, Wang Y, Zhang W, Zhou J, Shi B. Life cycle assessment for chrome tanning, chrome-free metal tanning, and metal-free tanning systems. ACS Sustain Chem Eng. 2021;9(19):6720–31. https://doi.org/10.1021/acssuschemeng.1c00753.
9. Shi J, Zhang R, Mi Z, Lyu S, Ma J. Engineering a sustainable chrome-free leather processing based on novel lightfast wet-white tanning system towards eco-leather manufacture. J Clean Prod. 2021;282:124504. https://doi.org/10.1016/j.jclepro.2020.124504.
10. Yu L, Qiang X, Cui L, Chen B, Wang X, Wu X. Preparation of a syntan containing active chlorine groups for chrome-free tanned leather. J Clean Prod. 2020;270:122351. https://doi.org/10.1016/j.jclepro.2020.122351.

11. Krishnamoorthy G, Sadulla S, Sehgal PK, Mandal AB. Green chemistry approaches to leather tanning process for making chrome-free leather by unnatural amino acids. J Hazard Mater. 2012;215–216:173–82. https://doi.org/10.1016/j.jhazmat.2012.02.046.
12. Izquierdo E, Robinet L, Boissière M, et al. Characterization of the effect of heat on vegetable tanned leather and restoration trials through enzymatic processes. In: The 5th international conference on advanced materials and systems. 2014. p. 517.
13. Kayaoğlu BK, Öztürk E. Imparting hydrophobicity to natural leather through plasma polymerization for easy care effect. Fiber Polym. 2013;14(10):1706–13. https://doi.org/10.1007/s12221-013-1706-y.
14. Xia Q, Yang L, Hu K, Li K, Xiang J, Liu G, Wang Y. Chromium cross-linking based immobilization of silver nanoparticle coating on leather surface with broad-spectrum antimicrobial activity and durability. ACS Appl Mater Inter. 2019;11(2):2352–63. https://doi.org/10.1021/acsami.8b17061.
15. Zhu R, Yang C, Li K, Yu R, Liu G, Peng B. A smart high chrome exhaustion and chrome-less tanning system based on chromium (III)-loaded nanoparticles for cleaner leather processing. J Clean Prod. 2020;277:123278. https://doi.org/10.1016/j.jclepro.2020.123278.
16. Gustavson KH. Chemistry of tanning processes. New York: Academic; 1956.
17. He X, Huang Y, Xiao H, Xu X, Wang Y, Huang X, Shi B. Tanning agent free leather making enabled by the dispersity of collagen fibers combined with superhydrophobic coating. Green Chem. 2021;23(10):3581–7. https://doi.org/10.1039/D1GC00380A.
18. Sun X, Jin Y, Lai S, Pan J, Du W, Shi L. Desirable retanning system for aldehyde-tanned leather to reduce the formaldehyde content and improve the physical-mechanical properties. J Clean Prod. 2018;175:199–206. https://doi.org/10.1016/j.jclepro.2017.12.058.
19. Bao Y, Zhang Y, Guo J, Ma J, Lu Y. Application of green cationic silicon-based gemini surfactants to improve antifungal properties, fiber dispersion and dye absorption of sheepskin. J Clean Prod. 2019;206:430–7. https://doi.org/10.1016/j.jclepro.2018.09.186.
20. Huang X, Kong X, Cui Y, Ye X, Wang X, Shi B. Durable superhydrophobic materials enabled by abrasion-triggered roughness regeneration. Chem Eng J. 2018;336:633–9. https://doi.org/10.1016/j.cej.2017.12.036.
21. Khosravi M, Azizian S. Synthesis of a novel highly oleophilic and highly hydrophobic sponge for rapid oil spill cleanup. ACS Appl Mater Inter. 2015;7(45):25326–33. https://doi.org/10.1021/acsami.5b07504.
22. Zhang Z, Liu H, Qiao W. Reduced graphene-based superhydrophobic sponges modified by hexadecyltrimethoxysilane for oil adsorption. Colloid Surface A. 2020;589: 124433. https://doi.org/10.1016/j.colsurfa.2020.124433.
23. Pang H, Chen Z, Gong H, Du M. Fabrication of a super hydrophobic polyvinylidene fluoride-hexadecyltrimethoxysilane hybrid membrane for carbon dioxide absorption in a membrane contactor. J Membr Sci. 2020;595: 117536. https://doi.org/10.1016/j.memsci.2019.117536.
24. Larmour IA, Bell SEJ, Saunders GC. Remarkably simple fabrication of superhydrophobic surfaces using electroless galvanic deposition. Angew Chem Int Ed. 2007;46(10):1710–2. https://doi.org/10.1002/anie.200604596.
25. Li S, Wang Y, Xu W, Shi B. Natural rubber-based elastomer reinforced by chemically modified multiscale leather collagen fibers with excellent toughness. ACS Sustain Chem Eng. 2020;8(13):5091–9. https://doi.org/10.1021/acssuschemeng.9b07078.
26. Iwasa J, Kumazawa K, Aoyama K, Suzuki H, Norimoto S, Shimoaka T, Hasegawa T. In situ observation of a self-assembled monolayer formation of octadecyltrimethoxysilane on a silicon oxide surface using a high-speed atomic force microscope. J Phys Chem C. 2016;120(5):2807–13. https://doi.org/10.1021/acs.jpcc.5b11460.
27. Liu B, Deng X, Xie Z, Cheng Z, Yang P, Lin J. Thiol–ene click reaction as a facile and general approach for surface functionalization of colloidal nanocrystals. Adv Mater. 2017;29(36):1604878. https://doi.org/10.1002/adma.201604878.
28. Zhou Y-Y, Song E-H, Deng T-T, Zhang Q-Y. Waterproof narrow-band fluoride red phosphor K_2TiF_6:Mn^{4+} via facile superhydrophobic surface modification. ACS Appl Mater Inter. 2018;10(1):880–9. https://doi.org/10.1021/acsami.7b15503.
29. Zhao M, Cao K, Liu M, Zhang J, Chen R, Zhang Q, Xia Z. Dual-shelled RbLi(Li_3SiO_4)2:Eu^{2+}@Al_2O_3@ODTMS phosphor as a stable green emitter for high-power LED backlights. Angew Chem Int Ed. 2020;132(31):13038–43. https://doi.org/10.1002/ange.202003150.
30. Xu L, Wang L, Shen Y, Ding Y, Cai Z. Preparation of hexadecyltrimethoxysilane-modified silica nanocomposite hydrosol and superhydrophobic cotton coating. Fiber Polym. 2015;16(5):1082–91. https://doi.org/10.1007/s12221-015-1082-x.
31. Yang W, Meyers MA, Ritchie RO. Structural architectures with toughening mechanisms in nature: a review of the materials science of type-I collagenous materials. Prog Mater Sci. 2019;103:425–83. https://doi.org/10.1016/j.pmatsci.2019.01.002.
32. Gautieri A, Vesentini S, Redaelli A, Buehler MJ. Hierarchical structure and nanomechanics of collagen microfibrils from the atomistic scale up. Nano Lett. 2011;11(2):757–66. https://doi.org/10.1021/nl103943u.
33. Shoulders MD, Raines RT. Collagen structure and stability. Annu Rev Biochem. 2009;78(1):929–58. https://doi.org/10.1146/annurev.biochem.77.032207.120833.
34. Du J, Huang C, Peng B. Influence of hydrophobic side chain structure on the performance of amphiphilic acrylate copolymers in leather-making. J Soc Leath Technol Chem. 2016;100(2):67–72.
35. Depalle B, Qin Z, Shefelbine SJ, Buehler MJ. Influence of cross-link structure, density and mechanical properties in the mesoscale deformation mechanisms of collagen fibrils. J Mech Behav Biomed. 2015;52:1–13. https://doi.org/10.1016/j.jmbbm.2014.07.008.
36. Shang X, Zhu Y, Li Z. Surface modification of silicon carbide with silane coupling agent and hexadecyl iodiele. Appl Surf Sci. 2017;394:169–77. https://doi.org/10.1016/j.apsusc.2016.10.102.

Publisher's Note